

# Ultrafast One-Pot Air Atmospheric Solution Combustion Approach To Fabricate Mesoporous Metal Sulfide/Carbon Composites with Enhanced Lithium Storage Properties

Yunhui Wang,<sup>†,‡,§,||,⊥</sup> Jing Zeng,<sup>†,‡,§,||,⊥</sup> Yueying Peng,<sup>†,‡,§,||</sup> Jiyang Li,<sup>†,‡,§,||</sup> Yiyong Zhang,<sup>†,‡,§,||</sup> He Li,<sup>†,‡,§,||</sup> and Jinbao Zhao<sup>\*,†,‡,§,||</sup>

<sup>†</sup>State Key Lab of Physical Chemistry of Solid Surfaces, Department of Chemical and Biological Engineering, College of Chemistry and Chemical Engineering, Xiamen University, Xiamen 361005, Fujian, China

<sup>‡</sup>Collaborative Innovation Center of Chemistry for Energy Materials, Department of Chemistry, College of Chemistry and Chemical Engineering, Xiamen University, Xiamen 361005, Fujian, China

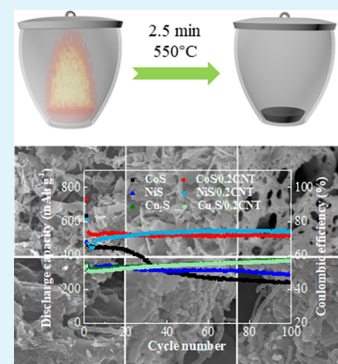
<sup>§</sup>State-Province Joint Engineering Laboratory of Power Source Technology for New Energy Vehicle, Xiamen University, Xiamen 361005, Fujian, China

<sup>||</sup>Engineering Research Center of Electrochemical Technology, Ministry of Education, Xiamen 361005, Fujian, China

## Supporting Information

**ABSTRACT:** The solution combustion synthesis (SCS) has been widely used to prepare varieties of materials, especially oxides. Nevertheless, there are just a few reports applying the SCS to synthesize sulfides, and most of them are prepared under the protection of an inert atmosphere. As the counterpart of metal oxides, the metal sulfides (MSs) also play an important role in energy-related devices. Herein, a novel air atmospheric SCS is proposed to prepare classes of MSs and the corresponding carbon composites. Thanks to the evaporation and flash burning of ethanol, the O<sub>2</sub> is consumed, protecting the MSs and the carbon nanotubes (CNTs) from oxidation; thus, the mesoporous CoS, NiS, Cu<sub>2</sub>S, and the CoS/CNT, NiS/CNT, Cu<sub>2</sub>S/CNT, can be easily and rapidly obtained by directly combusting in the air atmosphere. Compared to the conventional SCS for synthesizing the MSs, the equipment requirements of this proposed method are low, which is suitable for large-scale preparation. The lithium storage properties of MSs and MSs/CNTs are investigated, in which the MSs/CNT composites show excellent lithium storage performances. This work provides a promising method to facilely prepare sulfides and their composites for energy-related systems.

**KEYWORDS:** air atmospheric, solution combustion, metal sulfides, CNT, lithium batteries



## INTRODUCTION

The metal sulfides (MSs), owing to numerous electrochemical and photochemical properties, have been drawing great attention in different energy storage and conversion devices.<sup>1–5</sup>

On one hand, in the field of energy storage such as lithium and sodium batteries, besides the alloying materials, the multi-electron conversion metal sulfides are considered one of the next-generation anode materials due to their high specific capacities.<sup>6–11</sup> Compared to oxide counterparts, the MSs show higher electrical conductivity and are more kinetically favorable for redox reactions (the M–S bond is weaker than the M–O bond), leading to superior electrochemical performances.<sup>12</sup> On the other hand, various MSs are demonstrated as excellent electrocatalysts for hydrogen evolution reaction (HER), oxygen evolution reaction (OER), and oxygen reduction reaction (ORR) because of small Tafel slopes and low overpotentials.<sup>13</sup> Particularly, some MSs act as the bifunctional electrocatalysts for water splitting or photocatalysis.<sup>14,15</sup> Therefore, the MSs are deemed as the multifunctional materials in energy storage and conversion systems.

To obtain such MSs and the corresponding composites, numerous synthetic strategies have been explored, such as the hydro-/solvothermal method, spraying pyrolysis, ion exchange, electrospinning method, etc.<sup>16–19</sup> In some cases, an expensive customized apparatus, such as high-pressure reactor, high-voltage electrospinning device, and spray-drier apparatus, is demanded. In addition, annealing at high temperature and post-treatment are also required, which is time-consuming. All these disadvantages will hamper further application of MSs in such energy-related systems. In recent decades, the solution combustion synthesis (SCS) has captured increasing attention in synthesizing varieties of materials, owing to its advantages of time-efficiency, easy manipulating process, and low demand for equipment.<sup>20</sup> The number of related reports is continuously increasing, especially after 2004 (Figure S1a). Nevertheless, there are just a few (40 items) reports about preparing MSs

Received: July 26, 2018

Accepted: October 15, 2018

Published: October 15, 2018

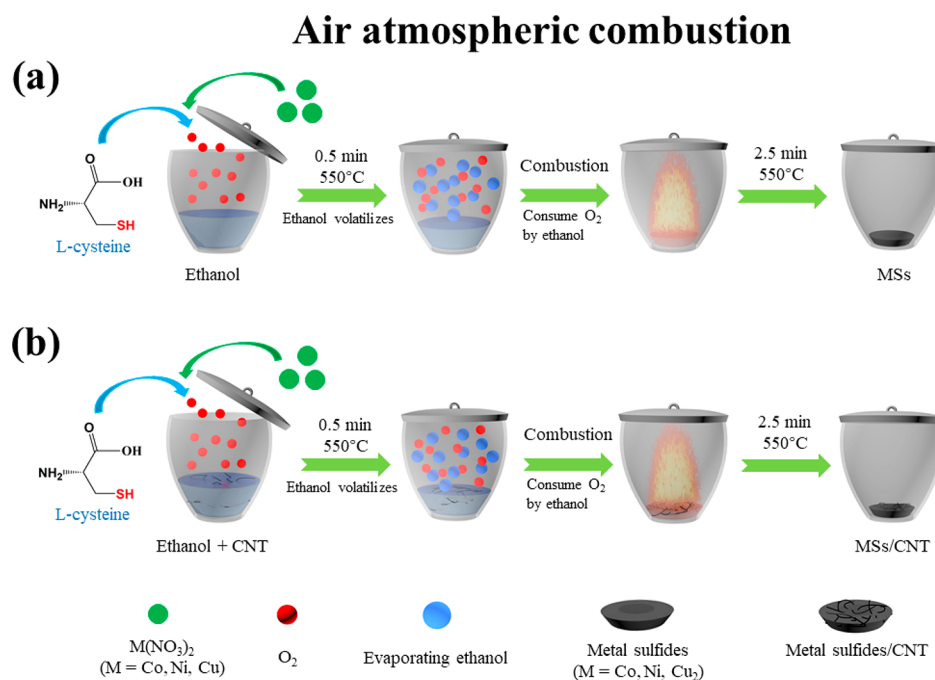


**Figure 1.** Proposed air atmospheric solution combustion synthesis of the (a) MSs and (b) MSs/CNT composites ( $M = \text{Co}, \text{Ni}, \text{and } \text{Cu}_2$ ).

and their composites (Figure S1b). The biggest problem is the high reactivity between sulfides and  $\text{O}_2/\text{H}_2\text{O}$  (in the air atmosphere) at high temperature; thus, instead of the MSs, the oxides are usually obtained if necessary protection measures are not taken.

To prepare targeted sulfides via the SCS, the most common strategy is the “inert atmosphere protection” strategy.<sup>21–23</sup> Tukhtaev and co-workers adopted this strategy to prepare different metal sulfides, such as  $\text{NiS}/\text{NiS}_2$  (admixture),  $\text{CoS}_2/\text{CoS}_{1.097}$ ,  $\text{Fe}_7\text{S}_8$ ,  $\text{Cu}_{1.8}\text{S}$ , and  $\text{ZnS}$ .<sup>22</sup> Boldyrev et al. prepared a class of metal sulfides ( $\text{NiS}$ ,  $\text{NiS}_2$ ,  $\text{CuS}$ , and  $\text{Cu}_{1.8}\text{S}$ , etc.). In these cases, the multistep synthetic processes are necessary. First, the thiourea/metal nitrate (or other thio-containing organics/metal nitrate) coordination precursors have to be elaborately prepared. Then the organic solvents are removed, and the precursors are pressed into tablets. Finally, the condensed tablets are heated and combusted in the tube furnace under the protection of an inert atmosphere. It is noted that the gas pressure and the rate of flow make significant differences in the crystal phases of the products. Otherwise, the admixtures such as  $\text{NiS}/\text{NiS}_2$  (admixture) and  $\text{CoS}_2/\text{CoS}_{1.097}$ , etc., are usually obtained instead of sulfide with the pure phase. Although the MSs can be prepared in this way, the advantages of SCS such as time-efficiency and easy manipulation process disappear, whereas the tedious preparation processes and rigorous experimental conditions hinder the application of the SCS in sulfides. Considering all aforementioned hardship, it seems to be a great challenge and also of great interest to explore a facile air atmospheric SCS to prepare metal sulfides and their carbon composites.

In this work, a novel air atmospheric SCS is proposed to fabricate classes of metal sulfides. Compared to the conventional SCS, this strategy not only inherits the aforementioned advantages (time-efficiency, easy manipulating and low demand for equipment) but also greatly reduces the interference of  $\text{O}_2/\text{H}_2\text{O}$  in the air, preparing the mesoporous MSs and MSs/CNT ( $M = \text{Co}, \text{Ni}, \text{and } \text{Cu}_2$ ) with high phase

purity. Directly combusting in the air, the MSs and MSs/CNT can be easily synthesized at high temperature ( $550\text{ }^\circ\text{C}$ ) via direct combustion in the air for 3 min. The lithium storage properties are evaluated, showing that the MSs/CNT composites display excellent electrochemical performances. We believe the proposed strategy can provide a new way to prepare both MSs and MSs/carbon composites for energy storage and conversion.

## EXPERIMENTAL SECTION

**Materials.** The  $\text{Co}(\text{NO}_3)_2 \cdot 5\text{H}_2\text{O}$  (Shanghai Sinopharm Reagent Chemical Co., Ltd.),  $\text{Ni}(\text{NO}_3)_2 \cdot 6\text{H}_2\text{O}$  (Guangdong Guanghua Sci-Tech Co., Ltd.),  $\text{Cu}(\text{NO}_3)_2 \cdot 3\text{H}_2\text{O}$  (Shantou Xilong Chemical Co., Ltd.), and L-cysteine (L-cys, J&K Chemical Co., Ltd.) were analytically pure. The carbon nanotubes (CNTs) were purchased from Chengdu Organic Chemicals Co., Ltd. All reagents were directly used without further purification.

**Synthesis of MSs and MSs/CNT Composites.** Typically, 2.0 mmol of metal nitrate ( $\text{Co}(\text{NO}_3)_2 \cdot 5\text{H}_2\text{O}$ ,  $\text{Ni}(\text{NO}_3)_2 \cdot 6\text{H}_2\text{O}$ , or  $\text{Cu}(\text{NO}_3)_2 \cdot 3\text{H}_2\text{O}$ , respectively) was added into a 50 mL crucible with 10 mL of absolute ethanol, followed by magnetic stirring until the metal nitrate was thoroughly dissolved. The L-cys of a specific amount (3.0 mmol for  $\text{Co}(\text{NO}_3)_2$ , 4.0 mmol for  $\text{Ni}(\text{NO}_3)_2$ , and 2.0 mmol for  $\text{Cu}(\text{NO}_3)_2$ , respectively) was added to the above solution, followed by magnetic stirring for 20 min. The precursors were transferred to a preheated ( $550\text{ }^\circ\text{C}$ ) muffle and remained there for 3 min. Then, the crucible was taken out and cooled down to room temperature. Finally, the  $\text{CoS}$ ,  $\text{NiS}$ , and  $\text{Cu}_2\text{S}$  were obtained without any post-treatment. The fabrication processes of the MSs/CNT were the same as those of MSs, except that 0.02 g of CNT was added to absolute ethanol, followed by addition of metal nitrate.

**Physical Characterization.** The microstructure and crystal nature were characterized by scanning electron microscope (SEM, Hitachi S-4800), transmission electron microscope (TEM, JEOL-2100), and X-ray powder diffractometer (XRD, Rigaku mini Flex 600 with  $\text{Cu } K\alpha$  radiation). The specific surface area was measured by  $\text{N}_2$  adsorption and desorption isotherms (the Micromeritics ASAP 2020 analyzer) and calculated via the Barret–Joyner–Halenda (BJH) method. The content of carbon was ascertained by element analysis (Vario EL III).

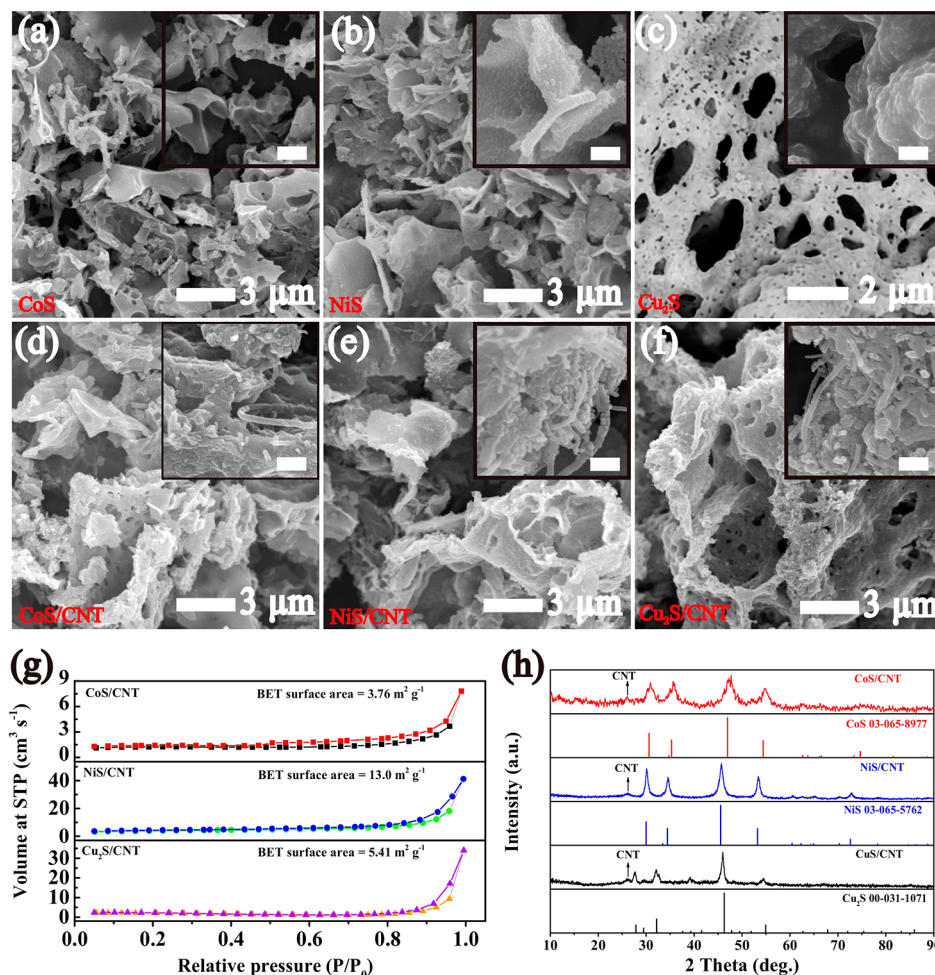


**Figure 2.** SEM images of (a) CoS, (b) NiS, (c) Cu<sub>2</sub>S, (d) CoS/CNT, (e) NiS/CNT, and (f) Cu<sub>2</sub>S/CNT. (g) N<sub>2</sub> adsorption and desorption profiles of MSs/CNT composites. (h) XRD patterns of CoS/CNT, NiS/CNT, Cu<sub>2</sub>S/CNT, and corresponding standard patterns. The scale bars of insets are all 300 nm.

**Electrochemical Measurements.** The lithium storage properties were investigated by 2016 coin cells assembled in an argon-filled glovebox, using lithium metal foils as both reference and counter electrodes, and the Asahi Kasei material as the separator. Also, the working electrode was fabricated by coating the slurry (MSs or MSs/CNT/acetylene black/polyvinylidene fluoride = 80/10/10 wt %) on a copper foil current collector, followed by drying and being pouched into a round disk with a diameter of 12 mm. The mass loading of active material was between 1.1 and 1.4 mg cm<sup>-2</sup>. The electrolyte was composed of 1 M lithium bis(trifluoromethanesulfon)imide (LiTFSI) in 1,3-dioxolane (DOL) and dimethyl ether (DME) (1:1, v/v). The galvanostatic charge and discharge tests were conducted on the Neware battery system between 1.0 and 3.0 V. The cyclic voltammetry (CV) data was recorded by the CHI 1000 (Chenhua, Shanghai) from 1.0 to 3.0 V at 0.2 mV s<sup>-1</sup>, and the Metrohm electrochemical workstation (Autolab PGSTAT 302N) from 0.2 to 0.6 mV s<sup>-1</sup>. The electrochemical impedance spectra (EIS) were collected from the Solartron Modulab 1287A/1260 from 10<sup>-1</sup> to 10<sup>5</sup> Hz. The specific capacity was calculated on the basis of the mass of sulfides, and all electrochemical measurements were performed at room temperature.

**Calculation of Apparent Li<sup>+</sup> Chemical Diffusion Coefficients via CV with Different Scanning Rates.** On the basis of the Randles-Sevcik equation, the apparent chemical diffusion coefficient of Li<sup>+</sup> was calculated as follows:<sup>24,25</sup>

$$i_p = 0.4463n^{3/2}F^{3/2}AC\left(\frac{FvD}{RT}\right)^{1/2}$$

where  $i_p$  is the redox peak current,  $n$  stands for the transferred number of electrons ( $n = 2$ ),  $F$  indicates the Faraday constant ( $F = 96485$  C), and  $C$  and  $A$  are the concentration of Li<sup>+</sup> of the sulfide matrix ( $C = 3.61 \times 10^{-2}$  mol cm<sup>-3</sup>) and the working electrode area ( $A = 1.13$  cm<sup>2</sup>), respectively.  $v$  is the scanning rate.  $R$  represents the gas constant ( $R = 8.314$  J mol<sup>-1</sup> K<sup>-1</sup>), and  $T$  is the temperature ( $T = 298$  K).  $D$  stands for the diffusion coefficient.

## RESULTS AND DISCUSSION

The synthetic strategy of the MSs and MSs/CNT is illustrated in Figure 1. The metal nitrate is used as both metal source and oxidizer, and the L-cys serves as both sulfur source and fuel. Due to the two different gas-producing functional groups (–COOH and –NH<sub>2</sub>), the L-cys is helpful to produce a large amount of gas (CO<sub>2</sub> and NH<sub>3</sub>) when it burns at high temperature, leaving numerous pores in the combusted products.<sup>23</sup> Other important factors are the reaction temperature and time. The reaction temperature is high enough (550 °C) to ignite combustion reaction and carbonization. The reaction time is short enough to protect sulfides from further oxidation. As mentioned before, the reactivity between metal sulfides and O<sub>2</sub>/H<sub>2</sub>O is high at high temperature. Even if sulfides can be produced in the combustion process, they will be oxidized very soon. Therefore, absolute ethanol here is used not only as the dispersion medium, but also as the protective agent. At 550 °C, ethanol rapidly evaporates and fulfills the

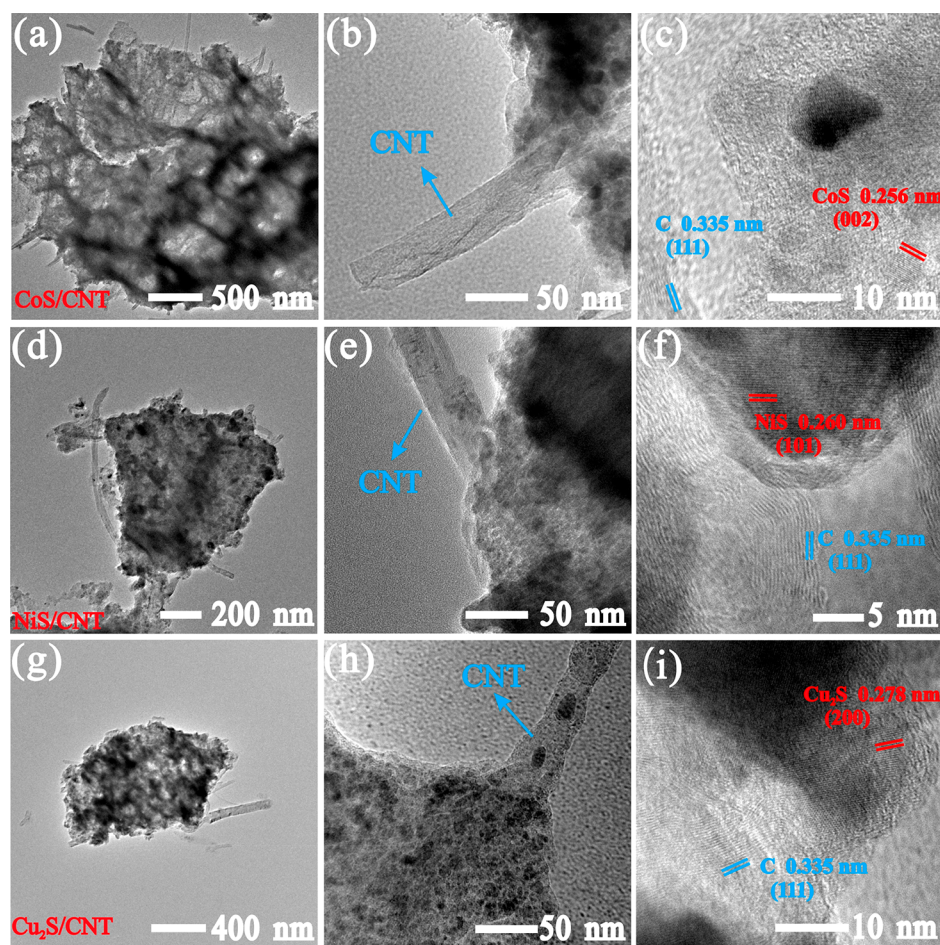


**Figure 3.** TEM images of (a–c) CoS/CNT, (d–f) NiS/CNT, and (g–i) Cu<sub>2</sub>S/CNT.

whole cavity of the crucible as well as the muffle. As it is continuously heated (very soon), the mixture will self-ignite as well as flash burn the gaseous ethanol, consuming most of the O<sub>2</sub>. In addition, the needed dosage of sulfur source (L-cys) in our strategy is far lower due to the good protection of ethanol (to be burning).

Thus, the metal sulfides can be produced in a dry and O<sub>2</sub>-free environment without the protection of an inert atmosphere. By taking advantage of the same strategy, MSs/CNT can also be successfully prepared, in which the CNT will not be burnt out by O<sub>2</sub> due to the protection of combustion of the ethanol.

The morphologies of the MSs and MSs/CNT are shown in Figure 2. The CoS and NiS powders are leaf-like, while Cu<sub>2</sub>S is coral-like with numerous voids/holes. The morphologies of CoS/CNT and NiS/CNT are similar to those of CoS and NiS. Fewer pores are observed in the case of Cu<sub>2</sub>S/CNT. The insets (Figure 2e,f) show that the twisted CNTs distribute inside/outside the sulfide matrix, indicating that the CNTs will not be burnt out in this strategy, or even combusted in the air atmosphere. The Brunauer–Emmett–Teller (BET) specific surface areas (SSAs) of CoS, NiS, and Cu<sub>2</sub>S are 2.06, 5.03, and 5.61 m<sup>2</sup> g<sup>-1</sup> (Figure S2), while those of CoS/CNT, NiS/CNT, and Cu<sub>2</sub>S/CNT are 3.76, 13.0, and 5.41 m<sup>2</sup> g<sup>-1</sup> (Figure 2g), respectively. The increased SSAs of CoS/CNT and NiS/CNT may be related with the emergence of mesopores and the increase of pore volume (Figure S3). The pore size distribution results show that a mesoporous structure exists in both the

MSs and the MSs/CNT. As illustrated before, the combustion of L-cys produces a large amount of CO<sub>2</sub> and NH<sub>3</sub> gases, leaving numerous pores. The elemental analysis (Table S1) shows that the weight contents of carbon in the CoS/CNT, NiS/CNT, and Cu<sub>2</sub>S/CNT are 25.1%, 26.4%, and 21.6%, respectively.

The crystal natures of the MSs are shown in Figure S4. The three combusted samples are identified as CoS (JCPDS 065-8977), NiS (JCPDS 065-5762), and Cu<sub>2</sub>S (JCPDS 031-1071), respectively. For the MSs/CNT, the diffraction patterns are the same as those of the MSs, wherein the peak intensity increases (Figure 2h). The emerging weak peak at 27° is indexed to the CNT. To further characterize the microstructures of the MSs/CNT, the TEM analysis is also conducted (Figure 3). The carbon nanotubes are clearly observed on the surfaces of MSs/CNT (Figure 3b,e,h), corresponding to the SEM results. The elemental mapping images (Figure S5) show that the elements sulfur, carbon, and the corresponding metal homogeneously distribute in the entire MSs/CNT composites. The high-resolution TEM (HRTEM) image (Figure 3c) shows that there are intersecting lattices. The lattice spacing of 0.256 nm is indexed to the (002) plane of CoS, and the twisted lattice with spacing of 0.335 nm is ascribed to the (111) plane of CNT. For the NiS/CNT and Cu<sub>2</sub>S/CNT, the twisted lattices belonging to CNTs are also observed, and the spacing of 0.260 and 0.278 nm corresponds to the (101) plane of NiS and the (200) plane of Cu<sub>2</sub>S, respectively. On the basis of the XRD, SEM, and TEM data, it can be concluded that the CNTs still

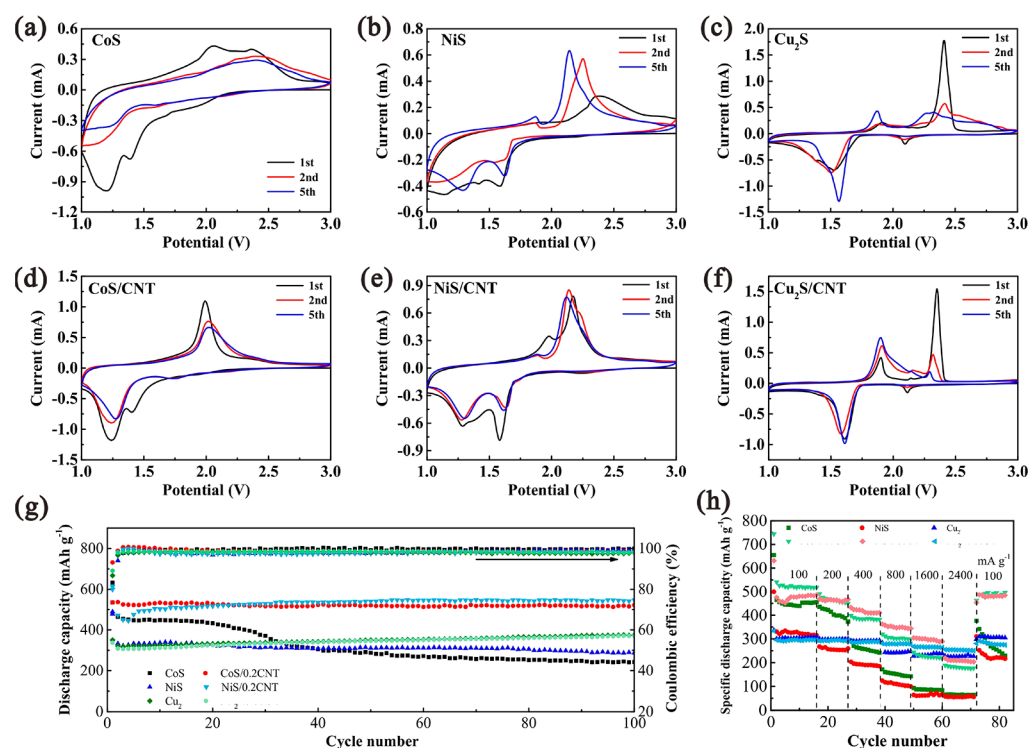


**Figure 4.** CV curves of (a) CoS, (b) NiS, (c) Cu<sub>2</sub>S, (d) CoS/CNT, (e) NiS/CNT, and (f) Cu<sub>2</sub>S/CNT at a scanning rate of 0.2 mV s<sup>-1</sup>. (g) Cycling performances of the MSs and MSs/CNT at 100 mA g<sup>-1</sup>. (h) Rate capability from 100 to 2400 mA g<sup>-1</sup>.

exist after combustion at 550 °C, and such MSs/CNT composites can be readily prepared by using this air-atmospheric solution combustion approach.

The lithium storage properties of the MSs and MSs/CNT are well-investigated. The CV curves of the MSs and the MSs/CNTs are shown in Figure 4a–f. In the first cycles, two pairs of redox peaks are observed. For CoS and CoS/CNT, the reduction peaks at ~1.4 and 1.2 V are related with the formation of the lithiated intermediate (LiCoS) and its further reduction to Co/Li<sub>2</sub>S, respectively. The oxidation peaks at ~2.0 and 2.4 V correspond to the inverse processes.<sup>26</sup> In the case of NiS and NiS/CNT, the CV profile in the first scan appears a little different, which may be related with the activation process. For NiS (Figure 4b), besides the reduction peak at 1.6 V, a broad peak between 1.1 and 1.4 V can be observed in the first scan due to the large electrochemical polarization (microsize and lacking the CNT conductive network). With subsequent scanning, two distinct reduction peaks at 1.3 and 1.7 V are observed, which are similar to those of NiS/CNT. For NiS/CNT, the polarization is weaker due to introduction of CNT. So, the two reduction peaks can be observed in the initial scan. The reduction peaks at ~1.7 and 1.3 V are ascribed to the decomposition of NiS to Ni<sub>3</sub>S<sub>2</sub>/Li<sub>2</sub>S and further reduction to Ni/Li<sub>2</sub>S, respectively.<sup>27,28</sup> The two oxidation peaks correspond to the regeneration of NiS.<sup>29</sup> For Cu<sub>2</sub>S, the reduction peaks at ~2.1 and 1.6 V are relevant to the reduction of residual copper sulfide to cuprous sulfide and reduction of Cu<sub>2</sub>S to Cu/Li<sub>2</sub>S, respectively.<sup>30,31</sup> The oxidation peaks at ~1.9 and 2.4 V are related to the formation of polysulfide intermediates and Cu<sub>2</sub>S, respectively.<sup>32</sup> Generally, the shapes of redox peaks of MSs/CNT are obviously more sharp and distinct than those of MSs. In addition, the gap between reduction and oxidation peaks is smaller for the MSs/CNT, indicating the higher electrochemical reversibility. The

galvanostatic charge and discharge plots are shown in Figure S6. The emerging (dis)charge plateaus agree with the results of the CV tests. The initial discharge capacity and Coulombic efficiency of MSs and MSs/CNT are shown in Table 1. The

**Table 1.** Initial Discharge Capacity and Coulombic Efficiency (CE)

	CoS	NiS	Cu <sub>2</sub> S
initial discharge capacity (mAh g <sup>-1</sup> )	632	478	350
Coulombic efficiency (%)	73.4	68.9	86.7
capacities after 100 cycles (mAh g <sup>-1</sup> )	242	287	374
	CoS/CNT	NiS/CNT	Cu <sub>2</sub> S/CNT
initial discharge capacity (mAh g <sup>-1</sup> )	732	614	337
Coulombic efficiency (%)	73.5	80.0	89.1
capacities after 100 cycles (mAh g <sup>-1</sup> )	521	546	370

releasing capacities of MSs/CNT are greatly improved, indicating the full use of active materials (the theoretical capacities of CoS, NiS, and Cu<sub>2</sub>S are 590, 590, and 337 mAh g<sup>-1</sup>, respectively, based on the two-electron conversion reaction). In addition, the Coulombic efficiencies are also increased, especially for NiS. The improved initial Coulombic efficiency indicates that more Li<sub>2</sub>S and metal can be charged back to the corresponding sulfides. As reported in our previous work, introducing CNTs as the interiorly conductive network actually helps to better utilize the active material.<sup>30</sup> After 50 cycles, the electrochemical polarization becomes pronounced, and the capacity significantly decays in the cases of CoS and NiS. It is well-known that metal sulfides are the conversion reaction-based materials, which suffer from great volume change during charging and discharging, especially for the micro-sized particles. The significant capacity drop after 50 cycles of CoS and NiS may be related with the electrode

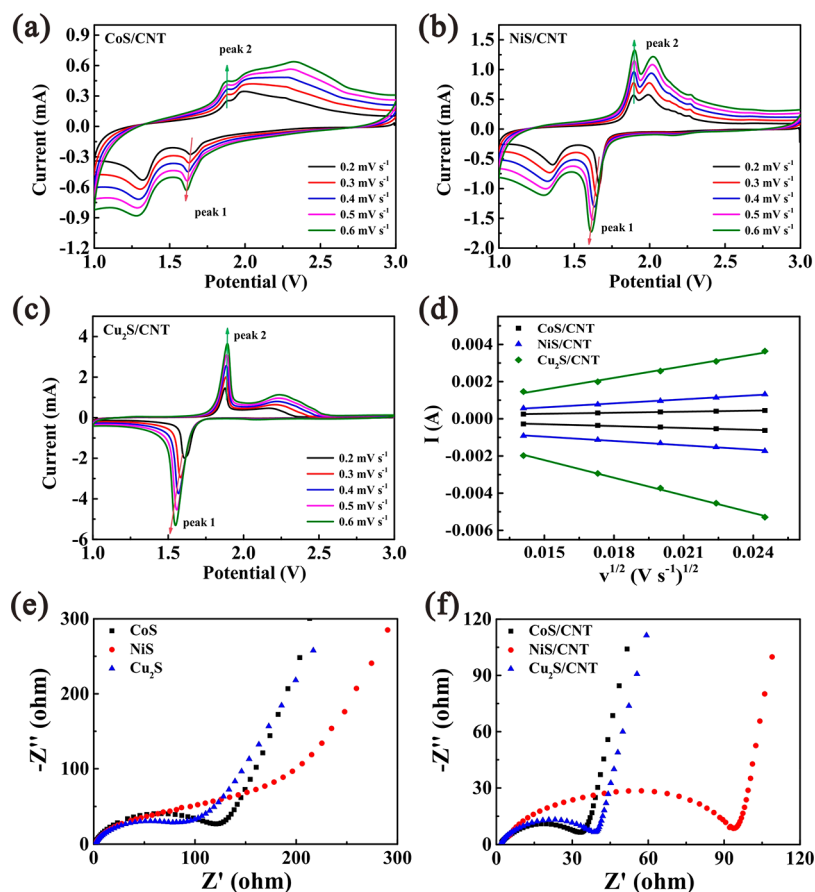


**Figure 5.** CV profiles of (a) CoS/CNT, (b) NiS/CNT, and (c) Cu<sub>2</sub>S/CNT at different scan rates and (d) relation between peak currents and the square root of scanning rates. EIS plots of (e) MSs and (f) MSs/CNT composite before cycling.

mechanical degradation. Nevertheless, for MSs/CNT, the degradation is inhibited since nanotubes could give great mechanical reinforcement due to the entangling structure.<sup>33,34</sup> Notably, the cycling stability and reaction reversibility of Cu<sub>2</sub>S seem not to be disturbed even without addition of the CNTs. The superior lithium storage property of Cu<sub>2</sub>S is ascribed to its intrinsic nature (high mobility of copper ions in the sulfide matrix, similarity of structure between Cu<sub>2</sub>S and Li<sub>2</sub>S, and low volume change during charge and discharge).<sup>35–37</sup>

The cycling performance is investigated at 100 mA g<sup>-1</sup>, as shown in Figure 4g. Overall, the reversible capacities of MSs/CNT composites are higher than those of the MSs. For the CoS and NiS, the effect of CNTs is more obvious, in which the capacity of CoS significantly fades after 25 cycles, and the reversible capacity of NiS is relatively low. After 100 cycles, the discharge capacities of CoS and NiS are 242 and 287 mAh g<sup>-1</sup>, respectively. Nevertheless, the CoS/CNT and NiS/CNT composites exhibit highly superior cycling reversibility, in which the releasing capacities after 100 cycles are 521 and 546 mAh g<sup>-1</sup>, respectively. Both Cu<sub>2</sub>S and Cu<sub>2</sub>S/CNT exhibit excellent cycling stability. The reversible capacities of MSs and MSs/CNT after 100 cycles are shown in Table 1. The rapid capacity fading of MSs is related to both volume change and loss of sulfur species. As the conversion reaction-based materials, the strong structural reorganization induces a large volume expansion, leading to particle pulverization and decohesion.<sup>38</sup> Besides, it is reported that the dissolution and diffusion of sulfur species also exist in the case of metal sulfides, causing capacity loss.<sup>39</sup> The two reasons cause the serious

capacity loss for the MSs. Nevertheless, for the MSs/CNT, the CNTs network not only serves as an electronic conductive network, but also as an elastic matrix to accommodate the mechanical stresses.<sup>40,41</sup> The volume expansion is well-accommodated, and the loss of sulfur species is greatly alleviated, leading to a greatly superior cycling stability of MSs/CNT. The rate capability is evaluated at different current densities (Figure 4h). The reversible capacities of CoS and NiS greatly decrease as the applied current density increases. At 2400 mA g<sup>-1</sup>, the releasing capacities of CoS and NiS are 69.4 and 57.5 mA g<sup>-1</sup>, respectively, whereas that of Cu<sub>2</sub>S can reach 225 mA h g<sup>-1</sup>. On the contrary, the reversible capacities of CoS/CNT, NiS/CNT, and Cu<sub>2</sub>S/CNT are 180, 207, and 255 mA h g<sup>-1</sup>, respectively. As the applied current is turned back to 100 mA g<sup>-1</sup>, the reversible capacities can be almost regained for the Cu<sub>2</sub>S and MSs/CNT, whereas both CoS and NiS show continuous capacity fading. From the above results, it can be known that introducing an interiorly conductive CNT network significantly improves not only the reversibility of the electrochemical reaction and cycling stability, but also the rate capability.

To understand the intrinsic function of the CNTs, the CV tests with different scanning rates are performed to investigate the kinetics of lithiation based on the Randles–Sevcik equation (Figure 5a–d and Figure S7) (see the Experimental Section), and the calculated diffusion coefficients are listed in Table 2. For the MSs, there is a huge difference in the diffusion coefficients among the metal sulfides, in which the diffusion coefficient of Cu<sub>2</sub>S is much higher than those of CoS and NiS.

**Table 2. Apparent Chemical Diffusion Coefficients of MSs and MSs/CNT**

	CoS	NiS	Cu <sub>2</sub> S
$D_{p1}$ ( $\times 10^{-12}$ cm <sup>2</sup> s <sup>-1</sup> )	0.1	2.34	195
$D_{p2}$ ( $\times 10^{-12}$ cm <sup>2</sup> s <sup>-1</sup> )	0.0351	1.98	149
	CoS/CNT	NiS/CNT	Cu <sub>2</sub> S/CNT
$D_{p1}$ ( $\times 10^{-12}$ cm <sup>2</sup> s <sup>-1</sup> )	1.18	6.23	831
$D_{p2}$ ( $\times 10^{-12}$ cm <sup>2</sup> s <sup>-1</sup> )	0.367	5.4	364

After complexation with the CNTs, the diffusion coefficients are further enhanced.

The coefficients of CoS/CNT are about 10-fold higher than those of CoS, and those of NiS/CNT are around 3-fold higher than those of NiS. Even for the Cu<sub>2</sub>S with desirable lithium storage properties, the effect of adding CNTs is also pronounced, in which the diffusion coefficients of Cu<sub>2</sub>S/CNT are 3-fold higher. Figure 5e,f shows the electrochemical impedance spectra of the MSs and MSs/CNT at the open circuit voltage (OCV), in which the semicircle indicates the general effect of electrical resistance and charge transfer rate.<sup>42</sup> The smaller semicircles of MSs/CNT indicate smaller electrical resistance and faster charge transfer. Thus, the improved rate capability of MSs/CNT can be well-explained by the enhanced kinetics of lithiation and decreased electrochemical impedance.

## CONCLUSION

In summary, a general and facile air atmospheric SCS is proposed to prepare a series of mesoporous MSs and MSs/CNT composites. Thanks to the evaporation and flash burning of ethanol, the O<sub>2</sub> is consumed, protecting the MSs and CNTs from oxidation. By using this strategy, the mesoporous CoS, NiS, Cu<sub>2</sub>S, and CoS/CNT, NiS/CNT, Cu<sub>2</sub>S/CNT with high phase purity can be rapidly and easily obtained. The lithium storage properties of MSs and MSs/CNT are investigated. After introducing CNTs as the interiorly conductive network, the lithium storage performances are significantly improved, and are investigated by the kinetics and electrochemical impedance analysis. We believe that this novel strategy can provide an alternative choice to prepare MSs and MSs/carbon composites for the energy storage and conversion.

## ASSOCIATED CONTENT

### Supporting Information

The Supporting Information is available free of charge on the ACS Publications website at DOI: 10.1021/acsae.8b01241.

Graphs of numbers of papers about combustion synthesis, N<sub>2</sub> adsorption and desorption profiles, pore size distribution, XRD patterns of metal sulfides (MSs), elemental mapping images of MSs/CNT, charge and discharge profiles, CV with different scanning rates of MSs, and elemental analysis results (PDF)

## AUTHOR INFORMATION

### Corresponding Author

\*E-mail: jbzhaoy@xmu.edu.cn.

### ORCID

He Li: 0000-0002-5324-8101

Jinbao Zhao: 0000-0002-2753-7508

## Author Contributions

<sup>†</sup>Y.W. and J.Z. share first authorship.

## Notes

The authors declare no competing financial interest.

## ACKNOWLEDGMENTS

The authors gratefully acknowledge the financial support of the National Natural Science Foundation of China (Grant 21621091) and National Key Research and Development Program of China (2017YFB0102000) and sincerely thank Prof. Daiwei Liao for his valuable suggestions.

## REFERENCES

- (1) Liu, Y.; Li, Y.; Kang, H.; Jin, T.; Jiao, L. Design, Synthesis, and Energy-related Applications of Metal Sulfides. *Mater. Horiz.* **2016**, *3*, 402–421.
- (2) Zhang, Y.; Zhou, Q.; Zhu, J.; Yan, Q.; Dou, S. X.; Sun, W. Nanostructured Metal Chalcogenides for Energy Storage and Electrocatalysis. *Adv. Funct. Mater.* **2017**, *27*, 1702317.
- (3) Zhang, X.; Cheng, X.; Zhang, Q. Nanostructured Energy Materials for Electrochemical Energy Conversion and Storage: A Review. *J. Energy Chem.* **2016**, *25*, 967–984.
- (4) Gao, M.; Xu, Y.; Jiang, J.; Yu, S. Nanostructured Metal Chalcogenides: Synthesis, Modification, and Applications in Energy Conversion and Storage Devices. *Chem. Soc. Rev.* **2013**, *42*, 2986–3017.
- (5) He, J.; Chen, Y.; Lv, W.; Wen, K.; Xu, C.; Zhang, W.; Li, Y.; Qin, W.; He, W. From Metal-Organic Framework to Li<sub>2</sub>S@C-Co-N Nanoporous Architecture: A High-Capacity Cathode for Lithium-Sulfur Batteries. *ACS Nano* **2016**, *10*, 10981–10987.
- (6) Yu, X.; David Lou, X. W. Mixed Metal Sulfides for Electrochemical Energy Storage and Conversion. *Adv. Energy Mater.* **2018**, *8*, 1701592.
- (7) Zhao, J.; Zhang, Y.; Wang, Y.; Li, H.; Peng, Y. The Application of Nanostructured Transition Metal Sulfides as Anodes for Lithium Ion Batteries. *J. Energy Chem.* **2018**, *27*, 1536.
- (8) He, J.; Li, P.; Lv, W.; Wen, K.; Chen, Y.; Zhang, W.; Li, Y.; Qin, W.; He, W. Three-dimensional hierarchically structured aerogels constructed with layered MoS<sub>2</sub>/graphene nanosheets as free-standing anodes for high-performance lithium ion batteries. *Electrochim. Acta* **2016**, *215*, 12–18.
- (9) He, J.; Lv, W.; Chen, Y.; Xiong, J.; Wen, K.; Xu, C.; Zhang, W.; Li, Y.; Qin, W.; He, W. Direct impregnation of SeS<sub>2</sub> into a MOF-derived 3D nanoporous Co–N–C architecture towards superior rechargeable lithium batteries. *J. Mater. Chem. A* **2018**, *6*, 10466–10473.
- (10) Xiong, X.; Wang, G.; Lin, Y.; Wang, Y.; Ou, X.; Zheng, F.; Yang, C.; Wang, J. H.; Liu, M. Enhancing Sodium Ion Battery Performance by Strongly Binding Nanostructured Sb<sub>2</sub>S<sub>3</sub> on Sulfur-Doped Graphene Sheets. *ACS Nano* **2016**, *10*, 10953–10959.
- (11) Zhang, Q.; Chen, H.; Luo, L.; Zhao, B.; Luo, H.; Han, X.; Wang, J.; Wang, C.; Yang, Y.; Zhu, T.; Liu, M. Harnessing the concurrent reaction dynamics in active Si and Ge to achieve high performance lithium-ion batteries. *Energy Environ. Sci.* **2018**, *11*, 669–681.
- (12) Xiao, Y.; Lee, S. H.; Sun, Y.-K. The Application of Metal Sulfides in Sodium Ion Batteries. *Adv. Energy Mater.* **2017**, *7*, 1601329.
- (13) Anantharaj, S.; Ede, S. R.; Sakthikumar, K.; Karthick, K.; Mishra, S.; Kundu, S. Recent Trends and Perspectives in Electrochemical Water Splitting with an Emphasis on Sulfide, Selenide, and Phosphide Catalysts of Fe, Co, and Ni: A Review. *ACS Catal.* **2016**, *6*, 8069–8097.
- (14) Zheng, M.; Ding, Y.; Yu, L.; Du, X.; Zhao, Y. In Situ Grown Pristine Cobalt Sulfide as Bifunctional Photocatalyst for Hydrogen and Oxygen Evolution. *Adv. Funct. Mater.* **2017**, *27*, 1605846.

- (15) Ranaweera, C. K.; Wang, Z.; Alqurashi, E.; Kahol, P. K.; Dvornik, P. R.; Gupta, B. K.; Ramasamy, K.; Mohite, A. D.; Gupta, G.; Gupta, R. K. Highly Stable Hollow Bifunctional Cobalt Sulfides for Flexible Supercapacitors and Hydrogen Evolution. *J. Mater. Chem. A* **2016**, *4*, 9014–9018.
- (16) Darr, J. A.; Zhang, J.; Makwana, N. M.; Weng, X. Continuous Hydrothermal Synthesis of Inorganic Nanoparticles: Applications and Future Directions. *Chem. Rev.* **2017**, *117*, 11125–11238.
- (17) Xia, X.; Zhu, C.; Luo, J.; Zeng, Z.; Guan, C.; Ng, C. F.; Zhang, H.; Fan, H. J. Synthesis of Free-standing Metal Sulfide Nanoarrays via Anion Exchange Reaction and Their Electrochemical Energy Storage Application. *Small* **2014**, *10*, 766–73.
- (18) Fei, L.; Williams, B. P.; Yoo, S. H.; Carlin, J. M.; Joo, Y. L. A General Approach to Fabricate Free-standing Metal Sulfide@carbon Nanofiber Networks as Lithium Ion Battery Anodes. *Chem. Commun.* **2016**, *52*, 1501–1504.
- (19) Zhu, Y.; Choi, S. H.; Fan, X.; Shin, J.; Ma, Z.; Zachariah, M. R.; Choi, J. W.; Wang, C. Recent Progress on Spray Pyrolysis for High Performance Electrode Materials in Lithium and Sodium Rechargeable Batteries. *Adv. Energy Mater.* **2017**, *7*, 1601578.
- (20) Varma, A.; Mukasyan, A. S.; Rogachev, A. S.; Manukyan, K. V. Solution Combustion Synthesis of Nanoscale Materials. *Chem. Rev.* **2016**, *116*, 14493–14586.
- (21) Tukhtaev, R. K.; Gavrilov, A. I.; Saveljeva, Z. A.; Larionov, S. V.; Boldyrev, V. V. The Effect of Nitrogen Pressure on the Synthesis of CdS From  $[\text{Cd}(\text{NH}_2\text{C}(\text{S})\text{NHNH}_2)_2](\text{NO}_3)_2$  Complex Compound Using Combustion Method. *J. Mater. Synth. Process.* **1999**, *7*, 19–22.
- (22) Tukhtaev, R. K.; Boldyrev, V. V.; Gavrilov, A. I.; Larionov, S. V.; Myachina, L. I.; Savel'eva, Z. A. Metal Sulfide Synthesis by Self-propagating Combustion of Sulfur-containing Complexes. *Inorg. Mater.* **2002**, *38*, 985–991.
- (23) Boldyrev, V. V.; Tukhtaev, R. K.; Gavrilov, A. I.; Larionov, S. V. On the Synthesis of Sulphides in Combustion Regime. *J. Therm. Anal. Calorim.* **2003**, *71*, 841–848.
- (24) Li, H.; Wang, Y.; Huang, J.; Zhang, Y.; Zhao, J. Microwave-assisted Synthesis of CuS/Graphene Composite for Enhanced Lithium Storage Properties. *Electrochim. Acta* **2017**, *225*, 443–451.
- (25) You, Y.; Yao, H. R.; Xin, S.; Yin, Y. X.; Zuo, T. T.; Yang, C. P.; Guo, Y. G.; Cui, Y.; Wan, L. J.; Goodenough, J. B. Subzero-Temperature Cathode for a Sodium-Ion Battery. *Adv. Mater.* **2016**, *28*, 7243–7248.
- (26) Gu, Y.; Xu, Y.; Wang, Y. Graphene-wrapped CoS Nanoparticles for High-capacity Lithium-ion Storage. *ACS Appl. Mater. Interfaces* **2013**, *5*, 801–6.
- (27) Fan, H.; Yu, H.; Wu, X.; Zhang, Y.; Luo, Z.; Wang, H.; Guo, Y.; Madhavi, S.; Yan, Q. Controllable Preparation of Square Nickel Chalcogenide (NiS and NiSe<sub>2</sub>) Nanoplates for Superior Li/Na Ion Storage Properties. *ACS Appl. Mater. Interfaces* **2016**, *8*, 25261–7.
- (28) Geng, H.; Kong, S. F.; Wang, Y. NiS Nanorod-assembled Nanoflowers Grown on Graphene: Morphology Evolution and Li-ion Storage Applications. *J. Mater. Chem. A* **2014**, *2*, 15152–15158.
- (29) Wang, Z.; Li, X.; Yang, Y.; Cui, Y.; Pan, H.; Wang, Z.; Chen, B.; Qian, G. Highly Dispersed  $\beta$ -NiS Nanoparticles in Porous Carbon Matrices by a Template Metal-organic Framework Method for Lithium-ion Cathode. *J. Mater. Chem. A* **2014**, *2*, 7912–7916.
- (30) Wang, Y.; Zhang, Y.; Li, H.; Peng, Y.; Li, J.; Wang, J.; Hwang, B.-J.; Zhao, J. Realizing High Reversible capacity: 3D intertwined CNTs inherently conductive network for CuS as an anode for lithium ion batteries. *Chem. Eng. J.* **2018**, *332*, 49–56.
- (31) Wang, Y.; Li, H.; Zhang, Y.; Peng, Y.; Zhang, P.; Zhao, J. Self-templating Thermolysis Synthesis of Cu<sub>2-x</sub>S@M (M = C, TiO<sub>2</sub>, MoS<sub>2</sub>) Hollow Spheres and Their Application in Rechargeable Lithium Batteries. *Nano Res.* **2018**, *11*, 831–844.
- (32) Wang, X.; Wang, Y.; Li, X.; Liu, B.; Zhao, J. A Facile Synthesis of Copper Sulfides Composite with Lithium-storage Properties. *J. Power Sources* **2015**, *281*, 185–191.
- (33) George, C.; Morris, A. J.; Modarres, M. H.; De Volder, M. Structural Evolution of Electrochemically Lithiated MoS<sub>2</sub> Nanosheets and the Role of Carbon Additive in Li-Ion Batteries. *Chem. Mater.* **2016**, *28*, 7304–7310.
- (34) Liu, Y.; He, X.; Hanlon, D.; Harvey, A.; Khan, U.; Li, Y.; Coleman, J. N. Electrical, Mechanical, and Capacity Percolation Leads to High-Performance MoS<sub>2</sub>/Nanotube Composite Lithium Ion Battery Electrodes. *ACS Nano* **2016**, *10*, 5980–90.
- (35) Débart, A.; Dupont, L.; Patrice, R.; Tarascon, J. M. Reactivity of transition Metal (Co, Ni, Cu) Sulphides versus Lithium: The Intriguing Case of the Copper Sulphide. *Solid State Sci.* **2006**, *8*, 640–651.
- (36) McDowell, M. T.; Lu, Z.; Koski, K. J.; Yu, J. H.; Zheng, G.; Cui, Y. In situ Observation of Divergent Phase Transformations in Individual Sulfide Nanocrystals. *Nano Lett.* **2015**, *15*, 1264–71.
- (37) Li, X.; He, X.; Shi, C.; Liu, B.; Zhang, Y.; Wu, S.; Zhu, Z.; Zhao, J. Synthesis of One-Dimensional Copper Sulfide Nanorods as High-Performance Anode in Lithium Ion Batteries. *ChemSusChem* **2014**, *7*, 3328–3333.
- (38) Cabana, J.; Monconduit, L.; Larcher, D.; Palacin, M. R. Beyond Intercalation-based Li-ion Batteries: The State of the Art and Challenges of Electrode Materials Reacting through Conversion Reactions. *Adv. Mater.* **2010**, *22*, E170–92.
- (39) Kalimuldina, G.; Taniguchi, I. Electrochemical Properties of Stoichiometric CuS Coated on Carbon Fiber Paper and Cu Foil Current Collectors as Cathode Material for Lithium batteries. *J. Mater. Chem. A* **2017**, *5*, 6937–6946.
- (40) Wang, J.; Lu, L.; Lotya, M.; Coleman, J. N.; Chou, S.; Liu, H.; Minett, A. I.; Chen, J. Development of MoS<sub>2</sub>-CNT Composite Thin Film from Layered MoS<sub>2</sub> for Lithium Batteries. *Adv. Energy Mater.* **2013**, *3*, 798–805.
- (41) Mao, W.; Ai, G.; Dai, Y.; Fu, Y.; Ma, Y.; Shi, S.; Soe, R.; Zhang, X.; Qu, D.; Tang, Z.; Battaglia, V. S. In-situ Synthesis of MnO<sub>2</sub>@CNT Microsphere Composites with Enhanced Electrochemical Performances for Lithium-ion Batteries. *J. Power Sources* **2016**, *310*, 54–60.
- (42) Zhou, W.; Zheng, J.; Yue, Y.; Guo, L. Highly Stable rGO-wrapped Ni<sub>3</sub>S<sub>2</sub> Nanobowls: Structure Fabrication and Superior Long-life Electrochemical Performance in LIBs. *Nano Energy* **2015**, *11*, 428–435.